

🍌 TACO: Training-free Sound Prompted Segmentation via Deep Audio-visual CO-factorization

Hugo Malard¹ Michel Olvera¹ Stéphane Lathuiliere¹ Slim Essid¹
¹LTCI, Télécom Paris, Institut Polytechnique de Paris
 hugo.malard@telecom-paris.fr

Abstract

Large-scale pre-trained audio and image models demonstrate an unprecedented degree of generalization, making them suitable for a wide range of applications. Here, we tackle the specific task of sound-prompted segmentation, aiming to segment image regions corresponding to objects heard in an audio signal. Most existing approaches tackle this problem by fine-tuning pre-trained models or by training additional modules specifically for the task. We adopt a different strategy: we introduce a training-free approach that leverages Non-negative Matrix Factorization (NMF) to co-factorize audio and visual features from pre-trained models to reveal shared interpretable concepts. These concepts are passed to an open-vocabulary segmentation model for precise segmentation maps. By using frozen pre-trained models, our method achieves high generalization and establishes state-of-the-art performance in unsupervised sound-prompted segmentation, significantly surpassing previous unsupervised methods.

1. Introduction

Audio-visual perception has attracted considerable interest due to its practical applications in various fields, especially robotics, video understanding [4, 39], and recently audio-visual language modeling [6, 25]. A particularly compelling task in this area is sound-prompted segmentation, which consists in pinpointing the image regions associated with sounds in a corresponding audio signal. Most approaches proceed to align audio and visual representations through contrastive learning techniques [30, 38, 41]. These techniques leverage paired audio-visual data to learn a shared embedding space, where corresponding audio and visual features are brought closer together, while non-corresponding pairs are pushed apart. The main challenge lies in learning local features that can be used for segmenting audio-related concepts, as videos typically provide global-level alignment (as opposed to local alignment

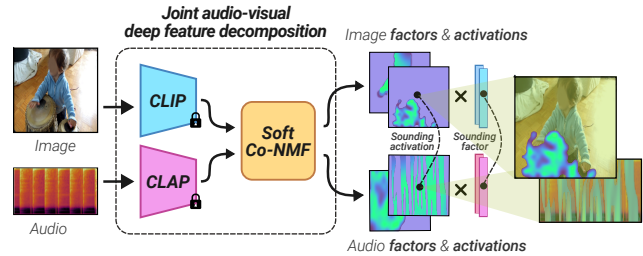


Figure 1. Our method takes a representation of an image and its associated audio as input, decomposing them into a product of 'semantic' factors and (spatial or temporal) activations. This decomposition enables locating parts of the original input corresponding to the concept present in both the image and the audio.

where each part of the image is matched with a part of the audio). More recently, a few works have made significant progress in this direction through the use of pre-trained models. For example, Park et al. [31] use a pre-trained CLIP encoder [32] and audio tokenizer within a relatively complex framework that translates audio signals into tokens compatible with CLIP's text encoder. This is combined with a grounding mechanism, enabling audio-driven segmentation of the image. Similarly, Hamilton et al.'s DenseAV [17] identifies image regions linked to sounds without supervision. Using a DINO image backbone [1] and the HUBERT audio transformer [19], it employs multi-head feature aggregation for contrastive learning on video-audio pairs.

While these approaches tackle sound-prompted segmentation through carefully designed architectures and dedicated training procedures, we propose a radically different strategy. Specifically, we ask: *can this task be addressed using only pre-trained audio and image models, without any task-specific training, by directly analyzing their feature representations?*

To answer this question, we introduce TACO: a *Training-free Audio-visual CO-factorization* approach, based on soft Non-negative Matrix co-Factorization (soft co-NMF) which identifies audio and visual tokens that are *co-activated* in the input signal. By leveraging pre-trained CLIP and CLAP

[10] backbones for image and audio, our co-NMF formulation enables audio-visual correspondence analysis without the need for training. Specifically, using a set of semantic *anchor words* projected into the CLIP and CLAP spaces, we are able to match audio features with visual ones in an interpretable fashion. Through simple inference-time optimization, our framework segments both visual and audio signals, performing object segmentation and sound localization in a training-free manner (illustrated in Figure 1). Furthermore, the interpretable factors identified by our decomposition framework allow us to directly prompt a pre-trained open-vocabulary segmenter, such as FC-CLIP [47], enhancing segmentation quality while remaining zero-shot.

Our approach stands out for its training-free paradigm and the interpretability offered by the NMF framework. Additionally, leveraging the robustness of the frozen CLIP and CLAP models enables us to achieve significantly superior performance compared to existing unsupervised training-based methods on established benchmarks. To summarize, our contributions are:

- We introduce TACO, the first training-free approach for sound-prompted segmentation based on pre-trained deep representations. Our framework leverages the inherent interpretability of NMF, enabling clear, semantically grounded visualization of interactions between segmentation outputs and the concepts identified within the signal.
- We enhance the quality of the segmentation provided by our co-NMF framework by incorporating a pre-trained open-vocabulary model (namely, FC-CLIP [47]), prompting its decoder with the most activated factors identified by our NMF system, for improved accuracy.
- We rigorously validate our approach through extensive experiments, providing both quantitative and qualitative analyses. We demonstrate the superior performance of our training-free approach across four datasets and multiple variants of the sound-prompted segmentation task. Additionally, the code used in our experiments will be released.

2. Related Work

2.1. Sound-Prompted Segmentation

Sound-prompted segmentation is the task of localizing in an image the object emitting the sound that is heard on an associated audio. Recent methods primarily utilize cross-modal attention for sound-prompted segmentation [35, 36, 42], often combined with a contrastive loss that learns to align audio and image global representations, hypothesizing that this process would implicitly foster the emergence of local alignment. Extending this contrastive learning framework, numerous enhancements have been introduced. These include integrating challenging negatives from background areas [3], adopting iterative contrastive learning

with pseudo-labels from earlier model epochs [22], maintaining transformation invariance and equivariance through geometric consistency [23], leveraging semantically similar hard positives [37], and implementing false negative-aware contrastive learning through intra-modal similarities [40].

Very recently, large pre-trained models have started to be used in order to benefit from their rich data representation. ACL-SSL [31] relies on the CLIP image encoder as well as a segmentation model CLIP-Seg[24], and learns an additional module that projects the audio in the CLIP space. Relying on DINO and HUBERT (further fine-tuned), Hamilton et al.[17] trained a multi-head module that identifies the localization of the sound in the image features.

Unlike these methods, our framework relies on a training-free setup leveraging pre-trained models and matrix decomposition. By avoiding training, our method not only avoids the need for a training dataset but also preserves the generalization abilities of the pre-trained model.

2.2. NMF and Deep Feature Factorization

Non-negative matrix factorization (NMF) has found applications in diverse fields, including audio source separation [15], document clustering [44], or face recognition [16], to mention a few. Previous research has expanded NMF to multiple layers [7], implemented NMF using neural networks [9], and utilized NMF approximations as inputs to neural networks[43]. More recently it has been applied to decompose deep neural features, for concept discovery [8], interpretability [27, 28] or audio-visual source separation [29]. While it has already been applied to co-factorize audio and visual (handcrafted) features [34], to the best of our knowledge this work is the first one to apply it to deep features for sound-prompted segmentation, as well as the first attempt to co-factorize representations from different spaces while enforcing semantic matching.

3. 🍷 TACO: Training-free Audio-visual CO-factorization

This section introduces our method, TACO, which allows training-free sound-prompted segmentation. Section 3.1 starts by presenting the main motivations. Section 3.2 provides the necessary background on NMF, and section 3.3 introduces our framework for extracting audio-visual concepts using NMF, while section 3.4 describes our complete solution for audio-source segmentation, which integrates our factorization approach into a pre-trained open-vocabulary image segmenter, enabling fine segmentation in a training-free manner.

3.1. Motivation

Our methodology leverages the capacity of recent large pre-trained models to effectively *localize* patterns within

their input signals [47]. *Localization* here refers to identifying spatial regions in images and temporal segments in audio. From this observation, we hypothesize that separately trained audio and visual encoders contain all the necessary information for sound-prompted segmentation without requiring additional training. To achieve this, we propose a method, TACO, which identifies concepts that co-activate across audio and image representations exploiting the Non-negative Matrix Factorization (NMF) framework [21]. NMF provides a training-free approach that jointly decomposes each signal into an activation matrix and a concept matrix. The activation matrix, in particular, can be interpreted as a segmentation matrix, highlighting regions of concept alignment.

Before detailing our approach, it is important to note that NMF is a tool that is meant to interpret input matrices composed of only non-negative values. The non-negativity constraints are key to the interpretability offered by the NMF framework. However, deep representations often include negative coefficients. To address this, a straightforward solution is to clip all negative values to zero, thus ensuring matrix non-negativity. Although this adjustment may result in some information loss, our preliminary experiments indicate that with backbones like CLIP [32] and CLAP [10], the representation power remains unaffected for our specific tasks and settings. Further experimental details on this are provided in Sec. 4.

3.2. Background

NMF Non-negative Matrix Factorization (NMF) [21] involves decomposing a non-negative matrix $X \in \mathbb{R}_+^{N \times C}$ into two non-negative matrices $U \in \mathbb{R}_+^{N \times K}$ and $V \in \mathbb{R}_+^{K \times C}$ such that $X \approx UV$. In typical machine learning applications of NMF [12], N represents the number of observations and C denotes the number of (non-negative) features per observation, while K is the rank of the factorization, controlling the number of *factors* or *components* into which the original matrix is decomposed. Assuming a measure of fit D is considered, NMF can be formulated as the following constrained optimization problem:

$$\min_{U, V \geq 0} D(X|UV). \quad (1)$$

As the V matrix is interpreted as the *factor* matrix, U corresponds to the *activations* of those factors.

Co-NMF extends the NMF framework to multiple data views analyzed in parallel. Assuming two data matrices $X_1 \in \mathbb{R}_+^{N \times C}$ and $X_2 \in \mathbb{R}_+^{N \times C}$ containing different modalities (such as audio and visual streams of a video), co-NMF exploits the mutual information shared between these modalities. It assumes that the different modalities share a common activation matrix U . In particular, [45, 46] decomposes these matrices into a shared activation matrix

$U \in \mathbb{R}_+^{K \times C}$ with view-specific factors $V_1 \in \mathbb{R}_+^{N \times K}$ and $V_2 \in \mathbb{R}_+^{N \times K}$. This formulation forces the activation matrix U to be consistent across both modalities, reflecting the intuition that events occurring in the audio also happen in the same time in the image stream. Although the factors are encoded in different spaces, they should remain the same. Formally, assuming measures D_1 and D_2 , and weighting hyperparameters $\beta_1 > 0$, $\beta_2 > 0$, co-NMF solves the following problem:

$$\min_{U, V_1, V_2} \beta_1 D_1(X_1|UV_1) + \beta_2 D_2(X_2|UV_2), \quad (2)$$

subject to non-negativity constraints on U , V_1 , and V_2 .

Note that, as there might be some temporal shift between the audio and image events, enforcing the same U matrix for both decompositions can be overly restrictive. To mitigate this issue, soft non-negative Matrix Co-Factorization (**soft co-NMF**) [34] introduces two separate activation matrices and includes a penalty term to minimize their dissimilarity. It is obtained by solving the following optimization problem, with a penalty function P , and hyperparameter $\beta_p > 0$

$$\min_{U_1, U_2, V_1, V_2} \beta_1 D_1(X_1|U_1V_1) + \beta_2 D_2(X_2|U_2V_2) + \beta_p P(U_1, V_1, U_2, V_2), \quad (3)$$

subject to non-negativity constraints on U_1 , U_2 , V_1 and V_2 .

3.3. Deep Non-negative Matrix co-Factorization

This section details how TACO leverages soft co-NMF to perform a zero-shot sound-prompted segmentation.

Soft co-NMF for token decomposition We assume access to an input video with a corresponding audio signal. For simplicity, let us initially consider the central frame of the video; we will later extend our approach to handle the entire video, incorporating the temporal dimension. Additionally, we assume the availability of trained audio and

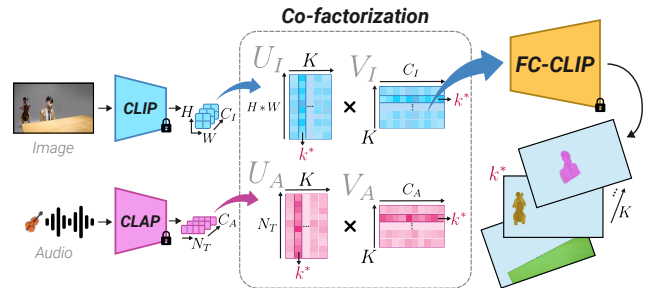


Figure 2. Complete pipeline: both the audio and the image are encoded using their respective encoder and their representations are used to perform the co-NMF. FC-CLIP is prompted using the image factors (V_I) and the segmentation corresponding to the sound-image factor ($V_I^{k^*}$) is kept as the final segmentation.

image backbones. Feeding the audio signal into the audio backbone produces a matrix $X_A \in \mathbb{R}_+^{N_T \times C_A}$, where N_T is the number of tokens, and C_A is the token dimension. Similarly, the image encoder maps an image to a feature representation $X_I \in \mathbb{R}_+^{H \times W \times C_I}$, where H and W represent the spatial dimensions, and C_I is the number of channels. Note that the spatial dimensions are flattened, resulting in a 2D matrix compatible with NMF inputs. Note that our approach diverges from prior works as the image activations encapsulate spatial, rather than temporal, information.

By applying soft co-NMF, we aim at factorizing X_A into matrices $U_A \in \mathbb{R}_+^{N_T \times K}$ and $V_A \in \mathbb{R}_+^{K \times C_A}$, along with X_I into $U_I \in \mathbb{R}_+^{H \times W \times K}$ and $V_I \in \mathbb{R}_+^{K \times C_I}$, where K denotes the predefined number of factors.

To enforce the non-negativity constraints in Eq. (3), we re-parameterize the problem using the sigmoid function σ and optimize matrices $\tilde{U}_A \in \mathbb{R}^{N_T \times K}$ and $\tilde{U}_I \in \mathbb{R}^{H \times W \times K}$, such that $U_A = \sigma(\tilde{U}_A)$ and $U_I = \sigma(\tilde{U}_I)$ with $U_I \in [0, 1]^{H \times W \times K}$ and $U_A \in [0, 1]^{N_T \times K}$. Restricting the decomposition to the interval $[0, 1]$ rather than \mathbb{R}_+ offers the advantage of an interpretable, well-calibrated scale. Specifically, the k -th column of U_I and U_A can be interpreted as the activation of the k^{th} factor for each token. In this way, the Hadamard product between the original tokens and a column of U_I or U_A can be viewed as soft masking, highlighting the portion of the original input that activates the k^{th} factor. Overall, those shifts lead us to challenge the existing soft co-NMF framework, proposing instead that audio and image factors should align, while activations may differ. Thus, we define a specific penalty function to impose semantic closeness between the factor matrices. As the modality-specific factors lie in different spaces, we introduce a new manner to ensure their semantic closeness.

Penalty function Applying soft co-NMF to a specific problem requires careful definition of the penalty term P in Eq. (3), as it impacts both the quality of the factorization and its interpretability. To achieve a semantically consistent factorization of audio-visual observations, P must effectively capture the semantic similarity between V_I and V_A . However, since the backbones (e.g., CLIP and CLAP) are not aligned, audio and image factors are encoded in two different subspaces, making L_1 or L_2 norms unsuitable as penalty functions. Moreover, audio and image representations are not necessarily commensurable: they often differ in dimensionality, precluding direct use of standard distances.

To address this, we propose projecting the audio and visual feature representations into a unified feature space to enable direct comparison. Specifically, we estimate aligned semantic descriptors \mathcal{D}_{I^k} and \mathcal{D}_{A^k} for the k^{th} column of U_I and U_A , respectively. These descriptors are computed using J semantic anchors, $\{b_I^j\}_{j=1}^J$ and $\{b_A^j\}_{j=1}^J$, which lie in the same spaces as X_I and X_A . Each anchor pair (b_I^j, b_A^j) rep-

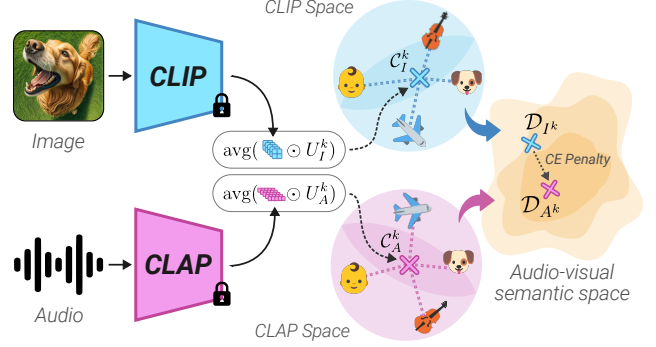


Figure 3. CLIP and CLAP encode audio and images in different spaces, complicating distance computation. Our method makes use of semantic anchors to project semantic components (pre-trained representations soft masked by the activations U_I^k and U_A^k obtained during the co-factorization) in an audio-visual semantic space where standard distances can be applied. Those distances are used as a penalty function during the decomposition to ensure that the audio and image concepts are the same.

resents a shared semantic concept, enabling the estimation of aligned semantic descriptors.

Specifically, to estimate aligned semantic anchors, we utilize CLIP [10] and CLAP [32] as image and audio backbones. Since these encoders are aligned with text encoders, we can exploit their respective text embeddings to align identical words across audio and image spaces. Thus, we define $b_I^j = \mathcal{E}_I(t_j)$ and $b_A^j = \mathcal{E}_A(t_j)$, where \mathcal{E}_I and \mathcal{E}_A are the text encoders of CLIP and CLAP, respectively, and $\{t_j\}_{j=1}^J$ represents a predefined word bank.

We now describe the process of estimating the semantic descriptors from the matrices U_A and U_I using the aligned semantic anchors. For simplicity, we detail only the estimation of semantic image descriptors; analogous steps apply to the audio descriptors.

First, we introduce *semantic components* \mathcal{C}_I^k associated to each column k of U_I . Since U_I^k represents the spatial activation of the k^{th} factor (corresponding to V_I^k), it can be interpreted as a soft segmentation mask for the input X_I . Applying these soft-masks to X_I and averaging the resulting representations extracts the concept associated with the k^{th} factor from the image features. Formally, the k^{th} image semantic component is computed as follows:

$$\mathcal{C}_I^k = \text{avg}(X_I \odot U_I^k), \quad (4)$$

where $\text{avg}(\cdot)$ denotes spatial average pooling (i.e. $f: \mathbb{R}^{H \times W \times C_I} \rightarrow \mathbb{R}^{C_I}$) and \odot is the Hadamard product. We define the semantic image descriptor \mathcal{D}_{I^k} by computing the

cosine similarity between \mathcal{C}_I^k and each semantic anchor:

$$\mathcal{D}_{I^k} = \begin{pmatrix} \cos(\mathcal{C}_I^k, b_I^1) \\ \vdots \\ \cos(\mathcal{C}_I^k, b_I^J) \end{pmatrix}, \quad (5)$$

where $\cos(\cdot)$ denotes cosine similarity. Intuitively, a descriptor quantifies the alignment of the semantic component with each semantic anchor (illustrated in Figure 3).

Note that V_I^k could have been used to play the role of semantic components instead of \mathcal{C}_I^k . However, V_I^k is less resilient to variations of the semantic anchors. Indeed, during the NMF optimization, V_I^k can take any range of values, potentially degenerating to values similar to those of b_I , which would be equivalent to performing a simple classification. In contrast, each \mathcal{C}_I^k is inherently constrained to be a weighted average of elements from the original representations, thus discouraging it from merely replicating values from b_I . We ablate this choice in Section 4.

Audio semantic descriptors \mathcal{D}_{A^k} are computed in the same way as their image counterparts. The penalty function is then defined as the cross-entropy between the image and audio semantic descriptors. However, enforcing similarity across all semantic descriptors may be detrimental, as certain semantic components may be visually present but inaudible, or vice versa. To address this, alignment is applied only to the closest audio and image semantic components. This choice is ablated in Section 4. Using the L_2 norm for reconstruction, we obtain V_A , V_I , U_A , and U_I by solving the following optimization problem:

$$\begin{aligned} \min_{V_A, V_I, U_A, U_I \geq 0} & [\beta_1 \|X_A - U_A V_A\|_2^2 \\ & + \beta_2 \|X_I - U_I V_I\|_2^2 \\ & + \beta_p \min_k \text{CE}(\mathcal{D}_{I^k}, \mathcal{D}_{A^k})], \end{aligned} \quad (6)$$

where CE denotes the cross-entropy function.

Interpretation After optimization, the k^{th} row of U_I represents the segmentation of the k^{th} factor in V_I (i.e. its k^{th} column) within the original image. The index k that realizes $\min_k \text{CE}(\mathcal{D}_{I^k}, \mathcal{D}_{A^k})$ corresponds to the dominant semantic component shared between the audio and image modalities, denoted as k^* . Consequently, row k^* of U_I , referred to as $U_I^{k^*}$, can be interpreted as the segmentation of the image region associated with the sound in the audio signal. Likewise, the segmentation of the spectrogram for this same semantic component is represented by $U_A^{k^*}$.

Temporal consistency To incorporate the temporal dimension in both the audio and visual inputs, if dealing with a video sequence, we introduce a temporal consistency regularization term in the decomposition process. Given a video, we extract T frames at a constant interval, and construct T audio-image pairs, denoted by $\{X_{A_t}\}_{t=1}^T$ and

$\{X_{I_t}\}_{t=1}^T$, by extracting the T consecutive non-overlapped audio frames centered around an image frame position. For each frame pair, we perform a decomposition into matrices $V_{A_t}, V_{I_t}, U_{A_t}, U_{I_t}$, introducing a regularization term \mathcal{R}_t to encourage consistency between the primary shared factors, $V_{I_t}^{k^*}$ and $V_{A_t}^{k^*}$, across consecutive frames. Formally, we add the following \mathcal{R}_t regularization term to the optimization objective of Eq. (6):

$$\mathcal{R}_t = -\beta_t \sum_{i=1}^T \cos(V_{I_t}^{k^*}, V_{I_{t+1}}^{k^*}) + \cos(V_{A_t}^{k^*}, V_{A_{t+1}}^{k^*}), \quad (7)$$

where $\beta_t \geq 0$ controls the temporal regularization.

3.4. Improved Segmentation with an Open Vocabulary Segmenter

Our soft co-NMF approach generates a segmentation mask for objects producing sound in the audio input through the k^* -th row of U_I . However, the segmentation accuracy is limited, as the CLIP features in the visual input X_I were trained only for image-level semantic alignment, not for precise segmentation. To enhance segmentation quality, we propose to integrate a pre-trained open-vocabulary segmentation model. To maintain compatibility with our NMF framework and keep the approach zero-shot, we select a model based on CLIP that preserves alignment with the text encoder without additional fine-tuning of the CLIP encoder. Here, we use the FC-CLIP model [47], which segments images using CLIP’s image encoder via text prompts encoded using the CLIP text encoder.

A valuable feature of FC-CLIP is its shared CLIP embedding space for both image and text inputs, which allows it to be prompted by vectors from the image space. Leveraging this, we prompt the FC-CLIP decoder with factors identified by our NMF framework. More precisely, in our soft co-NMF decomposition, the rows of matrix V_I represent the factors in the image space. Therefore, we can use them to prompt FC-CLIP, treating each factor in V_I as a segmentation class. Specifically, $V_I^{k^*}$ describes the shared “sounding” factor between audio and visual inputs.

Since $V_I^{k^*}$ resides in the CLIP space, it can also be compared to class name embeddings, allowing us to infer the segmented object’s class names and achieve *sound prompted image semantic segmentation*. The complete pipeline is depicted in Figure 2. Note that, incorporating FC-CLIP is computationally efficient, as the CLIP representation is computed only once before the soft co-NMF decomposition, with only the lightweight FC-CLIP decoder adding minor additional processing overhead (there is $\sim 200\text{M}$ parameters for the CLIP encoder and $\sim 20\text{M}$ for the FC-CLIP decoder).

4. Experimental protocol

Implementation details. To extract the modality-specific representations we utilize the MSCLAP 2023 [10] ($\sim 80\text{M}$ parameters) audio backbone and the OpenCLIP [5] ConvNeXt-Large CLIP trained on LAION 2B [33] ($\sim 200\text{M}$ parameters). For all experiments, we fix the decomposition coefficients to $\beta_I = \beta_2 = 1$, $\beta_p = 125$, and $K = 8$. For the temporal consistency constraint, we set the image and audio frame rate to one and use $\beta_t = 1$. However, since temporal consistency is specifically designed for single-source segmentation, we set $\beta_t = 0$ for the multi-source task. Those hyperparameters were selected based on preliminary experiments conducted on the AVSBench validation set. The optimization problem is solved using gradient descent in 1800 steps with a learning rate of 0.25. Importantly, the optimization process induces minimal computational overhead compared to the use of all pre-trained modules (details provided in the supplementary materials).

Datasets. We evaluate our method on five datasets: three for sound-prompted segmentation and two for sound-prompted semantic segmentation. For sound-prompted segmentation, we use: *AVS-Bench* [49], with binary segmentation maps for audio-visually related pixels, divided into single-source (S4, 5K samples) and multi-source (MS3, 400 samples) datasets. Additionally, we use *ADE20k sound-prompted* [17], which pairs ADE20k segmentation masks and images [48] with audio from VGGSound [2]. For sound-prompted semantic segmentation, we created *ADE Sound Prompted Semantic*: a semantic version of the ADE20k sound-prompted dataset, by assigning class labels to segmentation masks (detailed in supp. material). Moreover, we conduct experiments on *AVSS* [50], ($\sim 11\text{K}$ samples) comprising single and multi-source sounding objects. **Evaluation metrics.** We adopt standard segmentation metrics for evaluation: **mean** Intersection over Union (mIoU) and F-score for the semantic segmentation tasks, and mean Average Precision (mAP) as well as **mask** Intersection over Union (mask-IoU) and F-score for the binary segmentation tasks (we distinguish between mask and mean IoU to ensure comparability with previous works). Each experiment involving NMF decomposition was conducted three times, with the results reported as the average and standard deviation of the scores.

5. Results and Discussion

In this section, we compare our approach with other unsupervised methods tackling the task of sound-prompted segmentation. Most of the methods rely on fine-tuning (even if done unsupervisedly) which significantly modifies the original representations of pre-trained models. In contrast, our method is training-free and fully preserves the large generalization ability of the models it builds upon.

	ADE SP	S4	MS3	AVSS	ADE SP S.
A-FC-CLIP	45.31	51.52	33.67	11.95	24.95
A ⁺ -FC-CLIP	41.89	51.63	31.67	11.82	23.73

Table 1. Impact of clamping on the representation before feeding FC-CLIP. We report mIoU on five datasets. *ADE SP S.* corresponds to the ADE SP Semantic segmentation dataset. mask-IoU is reported for S4 and S3 and mIoU for all the other datasets.

For semantic segmentation, we use the class names provided with the dataset as the word bank. For non-semantic segmentation, no predefined class set is needed. We consider two variants of our method: in-domain segmentation, which uses a dataset-specific class set, and out-of-domain segmentation, which relies on a general set of 527 AudioSet[11] tags. For fair comparison, we report results using the general class list, unless otherwise noted.

Baseline. In the absence of prior work on unsupervised sound-prompted semantic segmentation, and to have a fair competitor that relies on the same pre-trained model, we consider a straightforward yet effective baseline approach: Audio-prompted-FC-CLIP (A-FC-CLIP). This method takes an audio input and its corresponding image, utilizing CLAP to determine the most likely class from the dataset’s class pool. FC-CLIP is then prompted to segment this class within the image. Note that for the baseline we use the dataset-specific class list as we use CLAP as a classifier that should rely on predefined class names.

Preliminary experiments: impact of clamping. To test the resilience of CLIP representations to clamping negative values, we experiment with FC-CLIP prompted only with the nonnegative part (via ReLU) of the CLIP text encoding, which is referred to as A⁺-FC-CLIP. Table 1 shows the performance degradation across all datasets. Except for the ADE SP dataset (~ 3.5 point drop), the decrease never exceeds 2 points. This experiment validates the use of clamping, enabling the application of NMF-based methods so as to benefit from their interpretability.

5.1. Sound-prompted Segmentation

We now discuss experiments on (non-semantic) Sound-Prompted Segmentation. Table 2 compares our approach with other unsupervised methods on the AVS-Bench, in both single and multi-source setups. TACO demonstrates strong performance relative to unsupervised training-based alternatives, outperforming the best competitor method by ~ 5 and ~ 9 points of mIoU in S4 and MS3 tasks. Our method also largely outperforms the A-FC-CLIP baseline that uses the same pre-trained models, underlining the effectiveness of our decomposition approach.

In the multi-source setup, while baseline performance drops substantially due to its limitation in handling only a single concept, our method shows robust performance. We

Method	S4			MS3	
	Training-free	mask-IoU \uparrow	F-Score \uparrow	mask-IoU \uparrow	F-Score \uparrow
SLAVC [26]	\times	28.10	34.60	24.37	25.56
MarginNCE [30]	\times	33.27	45.33	27.31	31.56
FNAC [38]	\times	27.15	31.40	21.98	22.50
Alignment [41]	\times	29.60	35.90	-	-
ACL-SSL [31]	\times	59.76	69.03	41.08	46.67
A-FC-CLIP	\checkmark	51.52	57.25	33.67	35.87
TACO	\checkmark	64.04 \pm 0.25	71.50 \pm 0.20	50.46 \pm 3.12	58.11 \pm 2.95

Table 2. Quantitative results of sound-prompted segmentation on the AVS-Bench test sets.

hypothesize that robustness arises because $V_I^{k^*}$ encodes information about **all** the sounding objects rather than just one, within the sounding factor. The hypothesis is explored qualitatively in Section 5.3.

Table 3 presents performance results on the recently proposed ADE Sound Prompted (ADE SP) dataset, along with variations of our approach on the same dataset to understand its gains. We compare existing methods with TACO variants, and our decomposition without FC-CLIP. Our experiments show that using $U_I^{k^*}$ alone from the decomposition leads to better segmentation of the image segments compared to previous audio-visual models. This is noteworthy since all competitors (like DenseAV [17], CAVMAE [14], DAVENet [18], and ImageBind [13]) are fine-tuned for this specific task. In contrast, we use frozen features, decompose them to identify matching factors, and demonstrate that these features contain the spatial information necessary for localization. Predictably, the use of FC-CLIP segmenter substantially refines the segmentation and the scores. Now, we examine the different variants of our approach to understand the large performance gap between TACO and existing methods. In the *TACO w/o component* variant, using V_I^k and V_A^k instead of the soft mask representations as semantic components during the optimization process (i.e., using $\mathcal{D}_I^k = V_I^k$ and $\mathcal{D}_A^k = V_A^k$) leads to degraded performance. In *TACO No-min*, we force all the concepts to be close, instead of only matching the closest, by using a penalty term where the min operator in (6) is replaced by an average. This results in a noticeable drop in performance. The last variant, *TACO w/o penalty*, shows the results using $\beta_p = 0$ (i.e., without penalization), which is equivalent to performing two independent decompositions and choosing $k^* = \operatorname{argmin}_k CE(\mathcal{D}_I^k, \mathcal{D}_A^k)$. As this decomposition is uni-modal, performance significantly drops.

Impact of the Word bank. Table 4 presents the mask-IoU scores on the three used sound-prompted segmentation datasets using either a general class list or one specific to the dataset. Using a specific class list overall improves both TACO results (+1 point on S4 and 3.5 points on ADE SP) and the segmentation using $U_i^{k^*}$ (+1 point on S4 and 5

	Segmenter	Training-free	m-IoU \uparrow	mAP \uparrow
DAVENet [18]	-	\times	17.0	16.8
CAVMAE [14]	-	\times	20.5	26.0
ImageBind [13]	-	\times	18.3	18.1
DenseAV [17]	-	\times	25.5	32.4
$U_I^{k^*}$ (Proposed)	-	\checkmark	27.74 \pm 0.48	35.75 \pm 0.33
A-FC-CLIP	FC-CLIP	\checkmark	45.31	50.36
TACO	No-min	\checkmark	29.93 \pm 1.95	34.59 \pm 3.17
	w/o component	\checkmark	22.70 \pm 0.74	23.68 \pm 2.03
	w/o penalty	\checkmark	26.75 \pm 0.14	30.17 \pm 0.12
	Proposed	\checkmark	51.57 \pm 0.86	60.01 \pm 1.38

Table 3. Quantitative results of sound-prompted segmentation on the ADE SP dataset.

points on ADE SP). On the multi-source MS3 dataset, the general class list performs better. This can be explained by the fact that, when multiple sound sources are present, a broader set of concepts can be beneficial, as one may align with the union of the sources (e.g., ‘Family’ could encompass both a woman and a baby making sounds).

5.2. Sound-Prompted Semantic Segmentation

Sound-Prompted Semantic Segmentation differs from Sound-Prompted Segmentation seen in the previous section as it requires the estimation of class labels corresponding to the mask. In TACO, classifying the audio prompt $V_I^{k^*}$ allows us to obtain the label of the segment. We run experiments on the AVSS and ADE20k sound-prompted semantic datasets. As shown in Table 5, our method greatly outperforms the baseline on the two datasets as it can take

	Word Bank	S4	MS3	ADE SP
$U_i^{k^*}$	General	27.78 \pm 0.06	28.20 \pm 0.61	32.42 \pm 0.74
	Specific	28.76 \pm 0.06	24.94 \pm 0.62	27.74 \pm 0.48
TACO	Specific	64.73 \pm 0.16	47.23 \pm 2.25	54.05 \pm 1.40
	General	64.04 \pm 0.25	50.45 \pm 3.12	51.57 \pm 0.86

Table 4. Comparison of the two word banks on sound-prompted segmentation datasets. mask-IoU is reported for S4 and MS3, while mIoU is reported for ADE SP.

Method	AVSS		ADE SP Semantic	
	mIoU \uparrow	F-Score \uparrow	mIoU \uparrow	F-Score \uparrow
A-FC-CLIP	11.95	13.56	20.91	24.95
TACO	20.50 \pm 0.10	23.02 \pm 0.09	37.70 \pm 1.61	44.39 \pm 1.92

Table 5. Quantitative results of sound-prompted semantic segmentation on the AVSS and ADE SP Semantic datasets.

advantage of both the image and the audio decompositions (+8 and 15 points of mIoU in AVSS and ADE SP Semantic, respectively). On the ADE SP Semantic, which contains a single class per image, the method performs well. However, on the AVSS dataset that contains samples with multiple classes, the performances drop. We attribute this to the class decoding process: since we estimate the class label as the closest one to the value of $V_I^{k^*}$, we consider the full segmentation as a single class. Nonetheless, the class-agnostic segmentation masks are accurate as the decomposition encodes all the concepts in a single vector (shown in supplementary materials).

5.3. Qualitative Analysis

Figure 4 shows images along with their associated $V_I^{k^*}$ reshaped as a matrix, the segmentation from TACO, and an illustration of the associated audio. The first row shows a challenging example from the S4 dataset where the sound source is nearly invisible, yet both TACO and $V_I^{k^*}$ successfully segment it. While recent works [20] underline how audio-visual segmenter models fail to deal with *negative audio* (i.e. audio depicting an event not present in the image), the second row illustrates the robustness of our method on that particular problem. As there is no common concept between the audio and image (given that the sound track of this example features music instead of the original audio recording of the scene), the estimated $V_I^{k^*}$ contains only noise, and as FC-CLIP does not find the concept, hence the final segmentation is empty, showing the resilience of TACO to those negative audios. Finally, the last row illustrates the case of multiple potential sources in the image. Even though the image features a Guitar, a Djembe, and singers, the model correctly segments only the people as only singing voice is heard on this excerpt.

Analysis in the Multi-Source setting. Figure 5 shows a segmentation example from the MS3 dataset as well as the similarity of the associated $V_I^{k^*}$ with some words. In the first row, the sound heard is a baby babbling, while the image contains both the baby, a woman, and a sofa. As expected, the closest word to $V_I^{k^*}$ “Baby babbling”, however, in the second row (next second of the video) both the women and the baby are emitting sound. As one might have expected that those two sounds were encoded in two different factors, it turns out that they both are encoded on the sounding factor $V_I^{k^*}$, as its similarity is maximal with

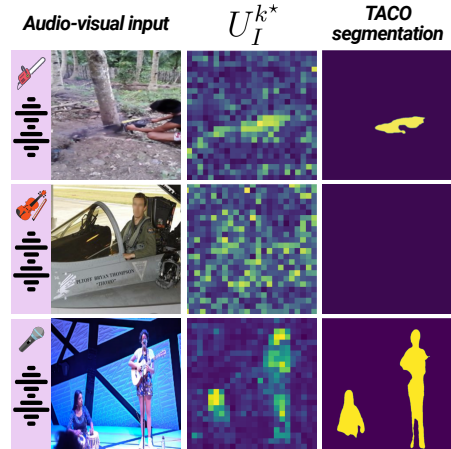


Figure 4. Qualitative segmentation examples from ADE SP and S4 datasets.

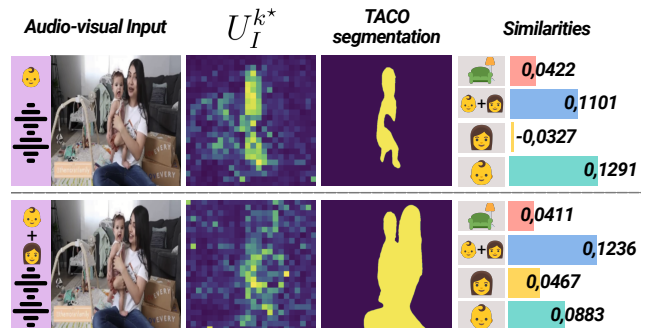


Figure 5. Multiple source segmentation examples. First row, a baby babbling is correctly segmented. Second row, the sounds of both a baby and a woman are encoded in a single factor showing that our decomposition encodes all sounding objects together.

“A baby babbling and a woman talking”, which is coherent with the segmentation. This observation enlightens our previous hypothesis made in section 5.1: the decomposition does not only encode one common concept between the audio and image features, but **all** the sounding objects, explaining its great performances in the multi-source task.

6. Conclusion

We introduced TACO, a method for training-free sound-prompted segmentation that effectively prompts an open vocabulary image segmentation model such as FC-CLIP with factors extracted through co-factorization of audio-visual deep embedding representations. Our method provides a framework for unsupervised sound-prompted segmentation, enabling the extraction and visualization of shared sounding concepts across audio spectrograms and image regions, which makes it inherently interpretable. TACO significantly outperforms concurrent unsupervised approaches, achieving state-of-the-art results.

References

- [1] Mathilde Caron, Hugo Touvron, Ishan Misra, Hervé Jégou, Julien Mairal, Piotr Bojanowski, and Armand Joulin. Emerging properties in self-supervised vision transformers. In *Proceedings of the IEEE/CVF international conference on computer vision*, 2021. 1
- [2] Honglie Chen, Weidi Xie, Andrea Vedaldi, and Andrew Zisserman. Vggsound: A large-scale audio-visual dataset. In *ICASSP 2020-2020 IEEE International Conference on Acoustics, Speech and Signal Processing (ICASSP)*. IEEE, 2020. 6
- [3] Honglie Chen, Weidi Xie, Triantafyllos Afouras, Arsha Nagrani, Andrea Vedaldi, and Andrew Zisserman. Localizing visual sounds the hard way. In *Proceedings of the IEEE/CVF conference on computer vision and pattern recognition*, 2021. 2
- [4] Sihan Chen, Handong Li, Qunbo Wang, Zijia Zhao, Mingzhen Sun, Xinxin Zhu, and Jing Liu. Vast: A vision-audio-subtitle-text omni-modality foundation model and dataset, 2023. 1
- [5] Mehdi Cherti, Romain Beaumont, Ross Wightman, Mitchell Wortsman, Gabriel Ilharco, Cade Gordon, Christoph Schuhmann, Ludwig Schmidt, and Jenia Jitsev. Reproducible scaling laws for contrastive language-image learning. In *Proceedings of the IEEE/CVF Conference on Computer Vision and Pattern Recognition*, 2023. 6
- [6] Sanjoy Chowdhury, Sayan Nag, Subhrajyoti Dasgupta, Jun Chen, Mohamed Elhoseiny, Ruohan Gao, and Dinesh Manocha. Meerkat: Audio-visual large language model for grounding in space and time. In *European Conference on Computer Vision*, pages 52–70. Springer, 2025. 1
- [7] Andrzej Cichocki, Rafal Zdunek, et al. Multilayer nonnegative matrix factorisation. *ELECTRONICS LETTERS-IEE*, 42(16), 2006. 2
- [8] Edo Collins, Radhakrishna Achanta, and Sabine Susstrunk. Deep feature factorization for concept discovery. In *Proceedings of the European Conference on Computer Vision (ECCV)*, 2018. 2
- [9] Gintare Karolina Dziugaite and Daniel M Roy. Neural network matrix factorization. *arXiv preprint arXiv:1511.06443*, 2015. 2
- [10] Benjamin Elizalde, Soham Deshmukh, Mahmoud Al Ismail, and Huaming Wang. Clap learning audio concepts from natural language supervision. In *ICASSP 2023-2023 IEEE International Conference on Acoustics, Speech and Signal Processing (ICASSP)*. IEEE, 2023. 2, 3, 4, 6
- [11] Jort F Gemmeke, Daniel PW Ellis, Dylan Freedman, Aren Jansen, Wade Lawrence, R Channing Moore, Manoj Plakal, and Marvin Ritter. Audio set: An ontology and human-labeled dataset for audio events. In *2017 IEEE international conference on acoustics, speech and signal processing (ICASSP)*. IEEE, 2017. 6
- [12] Nicolas Gillis. The why and how of nonnegative matrix factorization. *Regularization, optimization, kernels, and support vector machines*, 12(257), 2014. 3
- [13] Rohit Girdhar, Alaaeldin El-Nouby, Zhuang Liu, Mannat Singh, Kalyan Vasudev Alwala, Armand Joulin, and Ishan Misra. Imagebind: One embedding space to bind them all. In *Proceedings of the IEEE/CVF Conference on Computer Vision and Pattern Recognition*, 2023. 7
- [14] Yuan Gong, Andrew Rouditchenko, Alexander H Liu, David Harwath, Leonid Karlinsky, Hilde Kuehne, and James Glass. Contrastive audio-visual masked autoencoder. *arXiv preprint arXiv:2210.07839*, 2022. 7
- [15] Emad M Grais and Hakan Erdogan. Single channel speech music separation using nonnegative matrix factorization and spectral masks. In *2011 17th International Conference on Digital Signal Processing (DSP)*. IEEE, 2011. 2
- [16] David Guillamet and Jordi Vitria. Non-negative matrix factorization for face recognition. In *Catalonian Conference on Artificial Intelligence*. Springer, 2002. 2
- [17] Mark Hamilton, Andrew Zisserman, John R Hershey, and William T Freeman. Separating the” chirp” from the” chat”: Self-supervised visual grounding of sound and language. In *Proceedings of the IEEE/CVF Conference on Computer Vision and Pattern Recognition*, 2024. 1, 2, 6, 7
- [18] Wei-Ning Hsu, David Harwath, and James Glass. Transfer learning from audio-visual grounding to speech recognition. *arXiv preprint arXiv:1907.04355*, 2019. 7
- [19] Wei-Ning Hsu, Benjamin Bolte, Yao-Hung Hubert Tsai, Kushal Lakhota, Ruslan Salakhutdinov, and Abdelrahman Mohamed. Hubert: Self-supervised speech representation learning by masked prediction of hidden units. *IEEE/ACM transactions on audio, speech, and language processing*, 29, 2021. 1
- [20] Xavier Juanola, Gloria Haro, and Magdalena Fuentes. A critical assessment of visual sound source localization models including negative audio. *arXiv preprint arXiv:2410.01020*, 2024. 8
- [21] Daniel Lee and H Sebastian Seung. Algorithms for non-negative matrix factorization. *Advances in neural information processing systems*, 13, 2000. 3
- [22] Yan-Bo Lin, Hung-Yu Tseng, Hsin-Ying Lee, Yen-Yu Lin, and Ming-Hsuan Yang. Unsupervised sound localization via iterative contrastive learning. *Computer Vision and Image Understanding*, 2023. 2
- [23] Jinxiang Liu, Chen Ju, Weidi Xie, and Ya Zhang. Exploiting transformation invariance and equivariance for self-supervised sound localisation. In *Proceedings of the 30th ACM International Conference on Multimedia*, 2022. 2
- [24] Timo Lüddecke and Alexander Ecker. Image segmentation using text and image prompts. In *Proceedings of the IEEE/CVF conference on computer vision and pattern recognition*, 2022. 2
- [25] Hugo Malard, Michel Olvera, Stéphane Lathuilière, and Slim Essid. An eye for an ear: zero-shot audio description leveraging an image captioner with audio-visual token distribution matching. In *The Thirty-eighth Annual Conference on Neural Information Processing Systems*, 2024. 1
- [26] Shentong Mo and Pedro Morgado. A closer look at weakly-supervised audio-visual source localization. *Advances in Neural Information Processing Systems*, 2022. 7
- [27] Jayneel Parekh, Sanjeel Parekh, Pavlo Mozharovskiy, Florence d’Alché Buc, and Gaël Richard. Listen to interpret:

- Post-hoc interpretability for audio networks with nmf. *Advances in Neural Information Processing Systems*, 35, 2022. 2
- [28] Jayneel Parekh, Pegah Khayatan, Mustafa Shukor, Alasdair Newson, and Matthieu Cord. A concept-based explainability framework for large multimodal models. *arXiv preprint arXiv:2406.08074*, 2024. 2
- [29] Sanjeel Parekh, Slim Essid, Alexey Ozerov, Ngoc QK Duong, Patrick Pérez, and Gaël Richard. Guiding audio source separation by video object information. In *2017 IEEE Workshop on Applications of Signal Processing to Audio and Acoustics (WASPAA)*. IEEE, 2017. 2
- [30] Sooyoung Park, Arda Senocak, and Joon Son Chung. Marginnce: Robust sound localization with a negative margin. In *ICASSP 2023-2023 IEEE International Conference on Acoustics, Speech and Signal Processing (ICASSP)*. IEEE, 2023. 1, 7
- [31] Sooyoung Park, Arda Senocak, and Joon Son Chung. Can clip help sound source localization? In *Proceedings of the IEEE/CVF Winter Conference on Applications of Computer Vision (WACV)*, 2024. 1, 2, 7
- [32] Alec Radford, Jong Wook Kim, Chris Hallacy, Aditya Ramesh, Gabriel Goh, Sandhini Agarwal, Girish Sastry, Amanda Askell, Pamela Mishkin, Jack Clark, et al. Learning transferable visual models from natural language supervision. In *International conference on machine learning*. PMLR, 2021. 1, 3, 4
- [33] Christoph Schuhmann, Romain Beaumont, Richard Vencu, Cade Gordon, Ross Wightman, Mehdi Cherti, Theo Coombes, Aarush Katta, Clayton Mullis, Mitchell Wortsman, et al. Laion-5b: An open large-scale dataset for training next generation image-text models. *Advances in Neural Information Processing Systems*, 35, 2022. 6
- [34] Nicolas Seichepine, Slim Essid, Cédric Févotte, and Olivier Cappé. Soft nonnegative matrix co-factorization. *IEEE Transactions on Signal Processing*, 62(22), 2014. 2, 3
- [35] Arda Senocak, Tae-Hyun Oh, Junsik Kim, Ming-Hsuan Yang, and In So Kweon. Learning to localize sound source in visual scenes. In *Proceedings of the IEEE Conference on Computer Vision and Pattern Recognition*, 2018. 2
- [36] Arda Senocak, Tae-Hyun Oh, Junsik Kim, Ming-Hsuan Yang, and In So Kweon. Learning to localize sound sources in visual scenes: Analysis and applications. *IEEE transactions on pattern analysis and machine intelligence*, 43(5), 2019. 2
- [37] Arda Senocak, Hyeonggon Ryu, Junsik Kim, and In So Kweon. Learning sound localization better from semantically similar samples. In *ICASSP 2022-2022 IEEE International Conference on Acoustics, Speech and Signal Processing (ICASSP)*. IEEE, 2022. 2
- [38] Arda Senocak, Hyeonggon Ryu, Junsik Kim, Tae-Hyun Oh, Hanspeter Pfister, and Joon Son Chung. Sound source localization is all about cross-modal alignment. In *Proceedings of the IEEE/CVF International Conference on Computer Vision*, 2023. 1, 7
- [39] Ahmed Shahabaz and Sudeep Sarkar. Increasing importance of joint analysis of audio and video in computer vision: A survey. *IEEE Access*, 2024. 1
- [40] Weixuan Sun, Jiayi Zhang, Jianyuan Wang, Zheyuan Liu, Yiran Zhong, Tianpeng Feng, Yandong Guo, Yanhao Zhang, and Nick Barnes. Learning audio-visual source localization via false negative aware contrastive learning. In *Proceedings of the IEEE/CVF Conference on Computer Vision and Pattern Recognition*, 2023. 2
- [41] Weixuan Sun, Jiayi Zhang, Jianyuan Wang, Zheyuan Liu, Yiran Zhong, Tianpeng Feng, Yandong Guo, Yanhao Zhang, and Nick Barnes. Learning audio-visual source localization via false negative aware contrastive learning. In *Proceedings of the IEEE/CVF Conference on Computer Vision and Pattern Recognition*, 2023. 1, 7
- [42] Yapeng Tian, Jing Shi, Bochen Li, Zhiyao Duan, and Chenliang Xu. Audio-visual event localization in unconstrained videos. In *Proceedings of the European conference on computer vision (ECCV)*, 2018. 2
- [43] Thanh T Vu, Benjamin Bigot, and Eng Siong Chng. Combining non-negative matrix factorization and deep neural networks for speech enhancement and automatic speech recognition. In *2016 IEEE International Conference on Acoustics, Speech and Signal Processing (ICASSP)*. IEEE, 2016. 2
- [44] Wei Xu, Xin Liu, and Yihong Gong. Document clustering based on non-negative matrix factorization. In *Proceedings of the 26th annual international ACM SIGIR conference on Research and development in information retrieval*, 2003. 2
- [45] Naoto Yokoya, Takehisa Yairi, and Akira Iwasaki. Coupled nonnegative matrix factorization unmixing for hyperspectral and multispectral data fusion. *IEEE Transactions on Geoscience and Remote Sensing*, 50(2), 2011. 3
- [46] Jiho Yoo and Seungjin Choi. Matrix co-factorization on compressed sensing. In *Proceedings of the Twenty-Second international joint conference on Artificial Intelligence-Volume Volume Two*, 2011. 3
- [47] Qihang Yu, Ju He, Xueqing Deng, Xiaohui Shen, and Liang-Chieh Chen. Convolutions die hard: Open-vocabulary segmentation with single frozen convolutional clip. *Advances in Neural Information Processing Systems*, 36, 2023. 2, 3, 5
- [48] Bolei Zhou, Hang Zhao, Xavier Puig, Tete Xiao, Sanja Fidler, Adela Barriuso, and Antonio Torralba. Semantic understanding of scenes through the ade20k dataset. *International Journal of Computer Vision*, 127, 2019. 6
- [49] Jinxing Zhou, Jianyuan Wang, Jiayi Zhang, Weixuan Sun, Jing Zhang, Stan Birchfield, Dan Guo, Lingpeng Kong, Meng Wang, and Yiran Zhong. Audio-visual segmentation. In *European Conference on Computer Vision*. Springer, 2022. 6
- [50] Jinxing Zhou, Xuyang Shen, Jianyuan Wang, Jiayi Zhang, Weixuan Sun, Jing Zhang, Stan Birchfield, Dan Guo, Lingpeng Kong, Meng Wang, et al. Audio-visual segmentation with semantics. *International Journal of Computer Vision*, 2024. 6

🥥 TACO: Training-free Sound Prompted Segmentation via Deep Audio-visual CO-factorization

Supplementary Material

The supplementary material is organized as follows: the first part presents an analysis of the computations induced by the decomposition method, followed by an explanation of the metrics used and a comparison with other works. The last part consists of qualitative visualization and analysis of segmentation from TACO.

7. Computational overhead

The proposed NMF-based decomposition introduces additional computational costs compared to the baseline (consisting in prompting FC-CLIP with the predicted class from CLAP) as it requires optimization for each batch/sample. Figure 6 shows the performance (mAP) of TACO depending on the number of iterations in the optimization process as well as the associated relative computing time for a complete inference on the ADE SP test set. The performance plateaus after ~ 1000 iterations, which takes $\sim 20\%$ additional time compared to the baseline on a single Nvidia A100 80G.

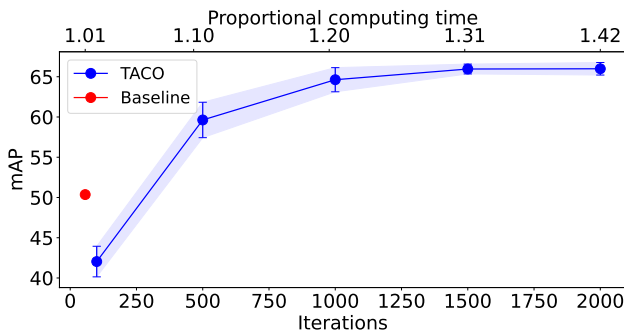


Figure 6. Proportion of additional computing time induced by the decomposition. The decomposition allows an improvement of ~ 12 points with only $\sim 20\%$ of additional compute time compared to the baseline.

8. Metrics discussion

Throughout this work, we reported mask-IoU as one of the primary metrics for sound-prompted segmentation on the AVSBench dataset, instead of mean-IoU. While mean-IoU is commonly used in segmentation tasks, it may not be the most appropriate metric in the context of binary segmentation. This is because mean-IoU averages the IoU of both the foreground and the background $(\text{IoU}(\text{foreground}) + \text{IoU}(\text{background}))/2$, potentially overemphasizing background accuracy, which is often less critical in binary tasks.

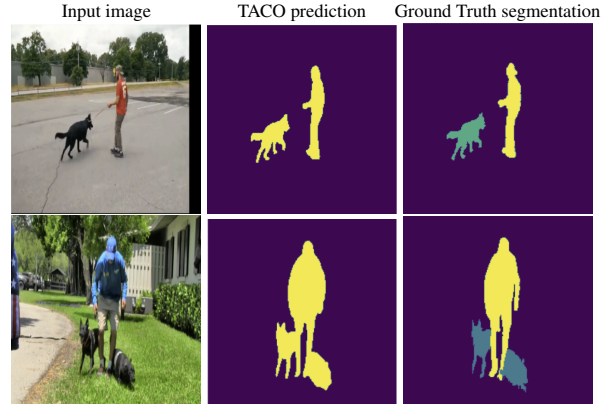


Figure 7. Semantic segmentation examples from AVSS.

In contrast, mask-IoU focuses solely on the IoU of the foreground, making it a more relevant and precise measure of segmentation quality in scenarios where the foreground object is the primary area of interest. However, we noticed that several works report mean-IoU in their papers, while in practice they measure mask-IoU. This discrepancy appears to stem from unintentionally replicating an error in the original repository of dataset AVSBench, which leads to potentially unfair comparisons between works. This discrepancy poses some challenges when comparing results, particularly for works without available code as the exact metric used cannot always be confirmed. Consequently, we were unable to compare our results with works for which the code was not available (like Bhosale et al.), as there was no assurance regarding the metrics used.

9. Semantic segmentation analysis

Figure 7 presents qualitative evidence supporting the hypothesis mentioned in Section 5.2: the semantic segmentation performance is hindered by the class inference process. Specifically, in a scenario with two sound sources, while both sources may be well segmented, each being encoded within the sounding concept through decomposition, the use of a single factor to infer the class leads to both sources being assigned the same class. This significantly penalizes the segmentation score.

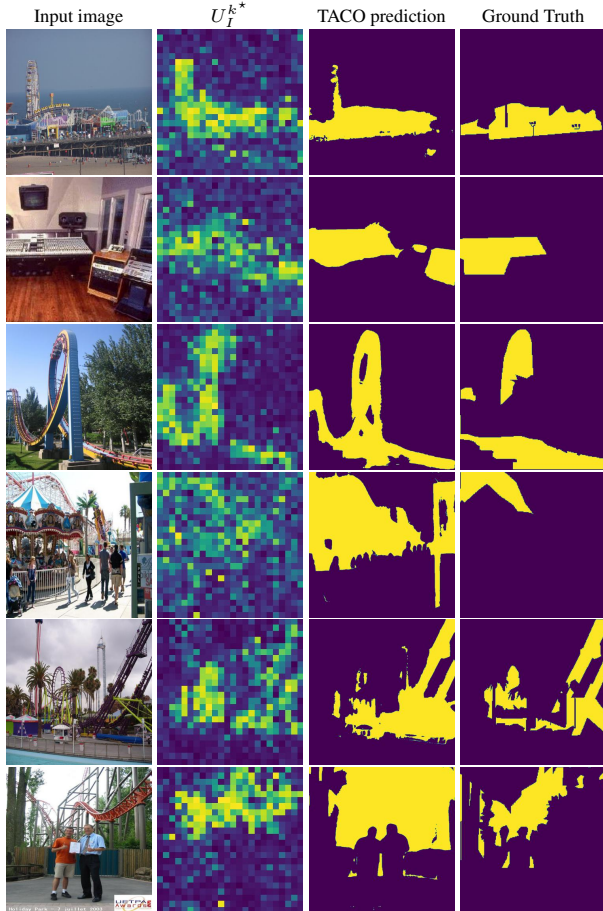


Figure 8. Sound-prompted segmentation examples from ADE SP.

10. Qualitative results of single and multiple sources, sound-prompted segmentation

Figure 8 presents randomly sampled segmentation examples from the ADE Sound prompted dataset, as well as their associated activation matrices U_I^{k*} , which enlightens the regions of the image that is used to extract the prompt to the segmenter model.

Figure 9 presents the equivalent analysis applied to the multi-sources dataset MS3.

11. Typical failure cases

Figure 10 shows typical failure cases of TACO. The first row depicts a case where the decomposition correctly identifies that the concept to segment is a piano (as shown by U_I^{k*}), but the segmenter model fails to clearly segment it, resulting in inaccurate segmentation. The second row shows an example where the decomposition fails to extract a clear concept, as it is unable to encode both audio concepts effectively, yielding partial and inaccurate segmentation. Finally, the third row highlights a special failure case where

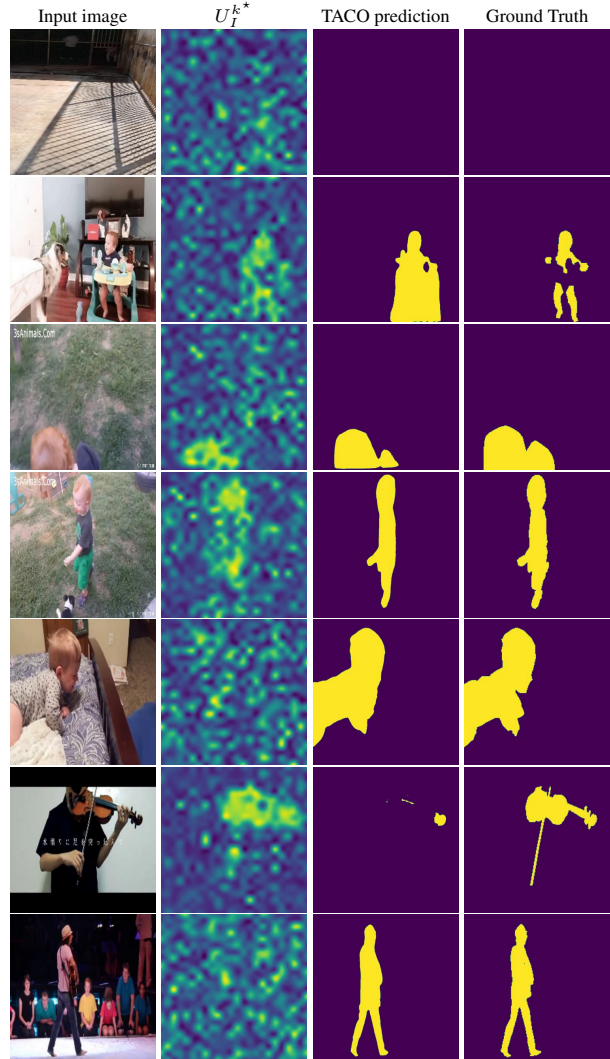


Figure 9. Sound prompted-segmentation examples from MS3.

the decomposition successfully encodes one concept but neglects the second. We hypothesize that this issue arises from limitations in the performance of the audio model (CLAP audio encoder).

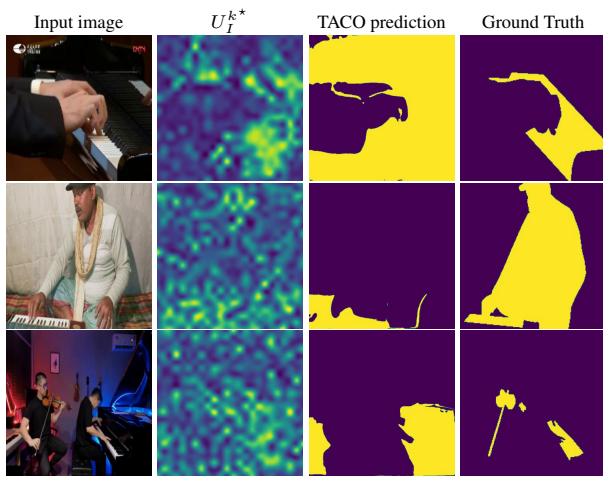


Figure 10. Examples of typical failure cases on MS3.